Crack Growth and Plastic Relaxation in a Drying Paste Layer

So KITSUNEZAKI[*]

Department of Physics, Graduate School of Human Culture, Nara Women's University, Nara 630-8506, Japan

Uniform drying causes a quasi-two-dimensional cellular crack pattern in a thin layer of paste. In our previous research, we found that such cracks are created in a capillary state, and that the growth speed is determined by the rate of increase in tension in the layer, rather than by the magnitude of the tension itself. In this paper, we present a theoretical investigation of the effects of increasing negative pore pressure and plastic deformation on crack growth using a modified spring network model. The analytical and numerical results indicate that the stress-rate dependence of crack speed could be caused by the competition between plastic relaxation and crack growth.

KEYWORDS: wet granular materials, paste rheology, mud crack patterns, crack growth speed, plastic deformation

1. Introduction

When a thin layer of paste is dried uniformly on a rigid plate, increased tension in the layer results in a familiar quasi-two-dimensional crack pattern. Cracks are generated sequentially during the middle stage of drying, and grow slowly at approximately constant speeds. The growth speed depends significantly on the material composition of the paste. For example, the range of speed was reported to be $0.2 - 2$ mm/min for mixtures of water and coffee powder,[1] and $2 - 200$ mm/s for cornstarch slurries.[2, 3] Although there have been numerous investigations of the formation of crack patterns in paste,[4] crack growth processes have not been sufficiently clarified.

Prior to crack formation, the drying paste used is in a semisolid state, and exhibits viscoplastic behavior. It fluidizes when stresses in excess of the yield stresses are applied.[5] Recent studies of the memory effect of paste indicated that rheological properties are important factors in fracture processes.[6–8]

Our previous experiments revealed that crack growth in paste is driven by tension increments.[9] In those experiments, a thin layer of fine calcium carbonate powder ($CaCO_3$) and water was dried from the open top surface at various drying rates. We measured the growth speeds of individual cracks from photographs, while the tensions arising in the layer were estimated from the deformation of a flat spring attached to the lateral boundary. The growth speed ranged from 5 to 50 mm/min and differed significantly among cracks generated at the same water volume fraction, while the tension was determined by the water volume fraction. The speed was found to be a nonlinear increasing function of the drying rate, or the rate of increase in the tension at the time of crack formation. No such dependence appears in pure viscoelastic materials. In a uniform layer of viscoelastic material subjected to gradually increasing tension, crack growth begins when a certain amount of elastic energy is stored, and accelerates to a speed determined by the tension. Although we were able to discuss some crack growth mechanisms in our previous work, especially the possibility of plastic relaxation in the vicinity of the crack tips, we were not able to ascertain the specific local processes involved.

In this paper, we take into account the fact that negative pore pressure on the free surface of paste can cause plastic relaxation as well as cracking. Such plastic relaxation can occur globally in a semi-soild paste. We devised a simple network model of rheological elements by modifying a spring network model to incorporate plasticity and negative pore pressure. The analytical and numerical results indicated that the drying rate dependence of crack growth could be caused by the competition between plastic relaxation and crack growth.

We focus on the growth of a semi-infinite straight crack in a paste layer with a uniform water distribution, and then introduce the model in the following sections. The analytical solution for steady crack growth under negligible yield stresses is derived in §5, and numerical results for finite yield stresses are presented in §6. A discussion and a summary of the conclusions drawn are presented in §7.

2. Rheological Model for a Paste Layer

Let us investigate a semi-infinite straight crack in a uniform paste layer of thickness h, as depicted in Fig. 1, where the crack grows in the x-direction and $X(t)$ indicates the crack tip position. Symmetry with respect to the x-axis is assumed, so that we need to consider only the half plane $y \geq 0$ in the analysis.

We begin by incorporating the effect of negative pore pressure into the free energy of the paste. Negative pore pressure increases while drying and induces contractions in the capillary state,[10–14] and the compressive stress $P(t)$ due to the pressure is supported by the granular structures on the free surfaces of the paste, as shown schematically in Fig. 2. We assume that the water distribution is uniform throughout the layer and neglect the effects of desiccation except with regard to increasing pore pressure, as there is only a slight decrease in the amount of water during the growth of a single crack. In this paper, $P(t)$ is regarded as a temporally increasing parameter with respect to drying.

Negative pore pressures are caused by the water-air interface on the free surfaces. Therefore, the sum of the interface energy F_i and the bulk energy of the paste F_b is equal to the entire free energy of the paste layer: $F \equiv F_b + F_i$. The changes in F_i and the paste volume v are related to $P(t)$ by $dF_i = Pdv$ when no crack forms. Pdv can be interpreted as the work per-
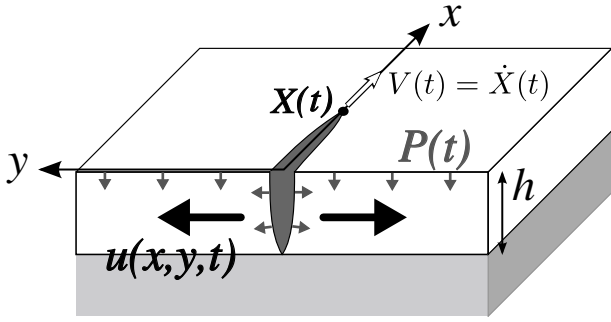
Fig. 1. Semi-infinite straight crack in a paste layer with a free top surface and a fixed bottom. $X(t)$ indicates the crack tip position and $V(t) \equiv \dot{X}(t)$ is the growth speed.
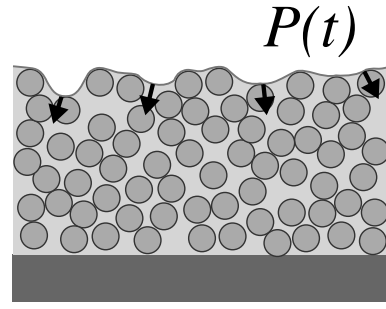

Fig. 2. Schematic of a capillary state of a paste and compressive stresses caused by negative pore pressures while drying.

formed on the bulk of the paste by the compressive stress. The granules and water in the paste are both practically incompressible for many types of paste. When the desiccation of water is negligible, the change in v is caused mainly by the invasion of air in the vicinities of the free surfaces.

As the crack growth creates new surfaces, when a crack is growing, we assume that $dF_i = Pdv + G_c h dX$, where G_c denotes the Griffith energy (the energy required to generate a unit area of crack surface). For irreversible crack growth, the interpretation of G_c should be extended to include the local dissipation energy at the crack tip, in accordance with standard fracture mechanics.[15]

F_b and v are functions of the state of the paste, $\mathcal{S}$, and the energy dissipation rate $\dot{F}$ is determined by the time derivative $\dot{\mathcal{S}}$. Thus, we assume that

$$\dot{F}(\mathcal{S}, \dot{\mathcal{S}}; X) = \dot{F}_b(\mathcal{S}; X) + P\dot{v}(\mathcal{S}; X) + hG_c\dot{X}, \qquad (1)$$

for paste with a crack, and this equation provides the basic formulation for the time development of $\mathcal{S}$ and X. In continuum theories of paste, $\mathcal{S}$ is generally described in terms of stresses and plastic strains. Plastic strains cause major deformations of paste in many instances, as the elastic strains are quite small owing to the weak yield stresses. We assume that plastic deformation is incompressible and consider only elastic volume changes.

In the following sections, we adopt a modified spring network model to construct F_b and v. The simplest dissipation function is used for $\dot{F}$, and elastic strains are used in place of stresses for convenience.

3. Modified Spring Network Model with Plasticity

We modify a spring network model to construct F_b and v. Spring network models represent a thin paste layer as a two-dimensional spring network connected to a fixed bottom by other springs, and springs that have been removed represent cracks. Such models have been used in numerous studies of mud crack patterns, although paste has generally been regarded as an elastic or viscoelastic material.[4] Figure 3 shows our network model composed of rheological elements, in which the layer is discretized into square meshes with a size $a_x \times a_y$ via $x_i = a_x i$ and $y_j = a_y(j - 1/2)$. For simplicity of analysis, the horizontal displacements are limited in the y-direction, and indicated by the scalar variables $u_{ij}(t)$. This model allows three strain modes for $u_{ij}(t)$ at a given point: shear strains in the x- and z-directions, and

dilation in the y-direction. We abbreviate these as $(\nabla u)_{ij} \equiv ((u_{i+1j} - u_{ij})/a_x, (u_{ij+1} - u_{ij})/a_y, u_{ij}/h)$.

Paste responds viscoelastically to small stresses due to repulsive interactions among granules. Assuming a linear elastoplastic decomposition, the elastic strains are expressed as $\mathbf{e}_{ij} \equiv (\nabla u)_{ij} - \mathbf{s}_{ij}$, where $\mathbf{s}_{ij} \equiv (s_{xij}, s_{yij}, s_{zij})$ indicates the plastic deformations corresponding to the three strain modes. On the basis of the assumption of linear elasticity, we set

$$F_b = \frac{1}{2} \sum_{ij}{}' a_x a_y h (\mu e_{xij}^2 + K e_{yij}^2 + \mu e_{zij}^2), \qquad (2)$$

where K and μ are the elastic coefficients for dilation and shear strains, respectively. The symbol $\sum'$ denotes the summation excluding the elements in the y-direction along the crack.

The paste volume is approximated by

$$v = \sum_{ij}{}' a_x a_y h e_{yij} + \text{const.}, \qquad (3)$$

taking into account elastic volume changes. We have not included the elastic dilation in the z-direction in eqs. (2) and (3), as it is independent of the horizontal displacements in spring network models.[4] The vertical displacements are considered implicitly, as plastic deformation has been assumed to be incompressible. This means that the layer thickness changes with s_{yij} to maintain the layer volume.

We derive the continuum limit of these equations in the x-direction as $a_x \to 0$, while retaining a discrete configuration in the y-direction to obtain the failure condition at the crack tip. To express these equations simply, we scale the coordinates and displacements using $x_i \to h x$, $y_j \to h' y_j$, and $u_{ij}(t) \to u u_j(x, t)$, respectively. Choosing $h' \equiv h\sqrt{K/\mu}$, eqs. (2) and (3) can be rewritten as

$$F_b = \frac{1}{2} \int dx \sum_j{}' a \mathbf{e}_j^2, \qquad (4)$$

$$v = \int dx \sum_j{}' a e_{yj} + \text{const.}, \qquad (5)$$

where $\mathbf{e}_j^2 \equiv e_{xj}^2 + e_{yj}^2 + e_{zj}^2$, $a \equiv a_y/h'$ and

$$\mathbf{e}_j \equiv \left(\frac{\partial u_j}{\partial x}, \frac{u_{j+1} - u_j}{a}, u_j \right) - \mathbf{s}_j. \qquad (6)$$

The other variables have been transformed according to $F_b \to \gamma h^2 F_b$, $v \to u h^2 v$, and $(h s_{xij}, h' s_{yij}, h s_{zij}) \to u \mathbf{s}_j(x, t)$, where
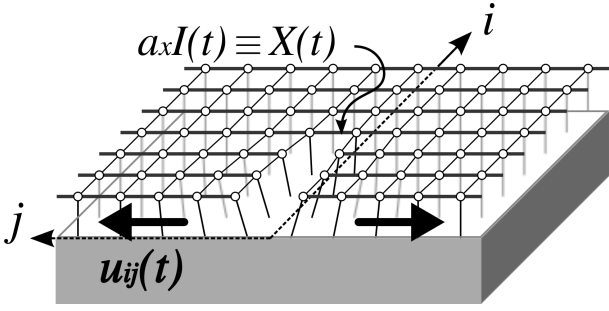
Fig. 3. Spring network model for a paste layer fixed at the bottom. A straight crack exists between $j = 0$ and 1 for $a_x i < X(t)$. The mesh size a_x in the x-direction vanishes in the continuum limit.

Fig. 4. Rheological elements at each site. The symbols X and Z denote elements similar to Y, composed of a spring and two dampers.

$\gamma \equiv (K\mu)^{\frac{1}{2}} u^2 / h$ is the unit of surface energy density. The scaling constant u can be chosen arbitrarily, and is used to simplify the failure condition in our numerical simulations. Equation (1) does not change, aside from replacing h with 1, since $X \to hX$, $P \to \gamma P / u$ and $G_c \to \gamma G_c$.

4. Time Development with Dissipation

We first assume the simplest quadratic form for dissipation:

$$\dot{F} = -\int dx \sum_j{}' a \left(\tau \dot{\mathbf{e}}_j^2 + \tau_p \dot{\mathbf{s}}_j^2 \right). \tag{7}$$

The first term describes viscous dissipation with a single relaxation time τ, and the second term corresponds to plastic dissipation with a relaxation time τ_p, where we have neglected the yield stresses of the paste. We can set $\tau = 1$ without the loss of generality by adopting τ as the unit of time. We may assume that $\tau_p \gg 1$, as plastic relaxation is markedly slower than viscous relaxation.

Equations (1) and (4)-(7) determine the time development of $u_j(x, t)$, $\mathbf{s}_j(x, t)$, and $X(t)$ for a given $P(t)$. After a cumbersome, but straightforward calculation (summarized in Appendix A), we can compare the coefficients of $\dot{u}_j$, $\dot{\mathbf{s}}_j$, and $\dot{X}$ individually, assuming that the boundary conditions for the region $y > 0$ are

$$\begin{cases} u_0(x, t) = -u_1(x, t) & \text{on the } x\text{-axis} \\ u_j(x, t) \to 0 & \text{for } x \to \infty \text{ or } j \to \infty \\ e_{xj}(x, t) \to 0 & \text{for } x \to -\infty \end{cases} \tag{8}$$

Introducing new variables $(U_j, \mathbf{S}_j) \equiv (1 + \partial/\partial t)(u_j, \mathbf{s}_j)$, we obtain the basic equations

$$\mathcal{L} U_j = \frac{\partial S_{xj}}{\partial x} + \frac{S_{yj} - S_{yj-1}}{a} - S_{zj} \quad \text{for } j > 1, \tag{9}$$

$$\tau_p \dot{\mathbf{s}}_j = \mathbf{f}_j \quad \text{for } j \geq 0, \tag{10}$$

with the stress boundary conditions on the x-axis given by

$$\sigma = \begin{cases} \dfrac{2U_1}{a} - S_{y0} & \text{for } x \geq X(t) \\ -P & \text{for } x \leq X(t) \end{cases}, \tag{11}$$

and the failure condition at the crack tip $x = X(t)$ given by

$$\frac{a}{4} \left(\frac{2u_1}{a} - s_{y0} + P \right)^2 = G_c'. \tag{12}$$

Here, we have defined $G_c' \equiv G_c + a^2 P^2 / 4$,

$$\mathcal{L} U_j \equiv \frac{\partial^2 U_j}{\partial x^2} + \frac{U_{j+1} + U_{j-1} - 2U_j}{a^2} - U_j, \tag{13}$$
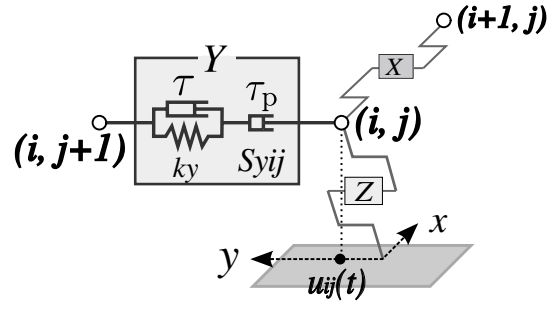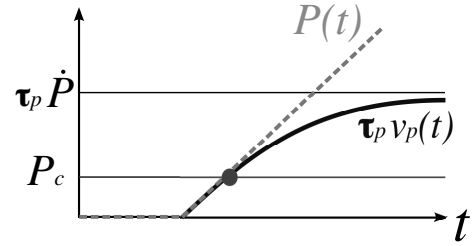

Fig. 5. Change in v_p in the case of a linearly increasing $P(t)$.

$$\mathbf{f}_j \equiv \left(\frac{\partial U_j}{\partial x}, \ \frac{U_{j+1} - U_j}{a} + P(t), \ U_j \right) - \mathbf{S}_j, \tag{14}$$

and

$$\sigma \equiv \frac{U_2 - U_1}{a} - S_{y1} + a \left(\frac{\partial^2 U_1}{\partial x^2} - \frac{\partial S_{x1}}{\partial x} - U_1 + S_{z1} \right). \tag{15}$$

Equations (9) and (10) are equivalent to the rheological model composed of three mechanical elements, a spring and two dampers, shown in Fig. 4. Viscous dissipation causes the relaxation of u_j toward a natural elastic state U_j determined by the semidiscrete Helmholtz equation eq.(9). On the other hand, plastic deformation, described by eq. (10), causes the relaxation of $\mathbf{s}_j$ toward the state $(1 + \partial/\partial t)\mathbf{e}_j = (0, -P(t), 0)$, which is an isotropic stress state, since the paste layer is also subjected to the vertical compressive stress $P(t)$.

The failure condition eq. (12) is obtained because discreteness in the y-direction prevents a stress singularity at the crack tip. We infer that such discreteness is essentially caused by grains in the paste, and a is the order of the magnitude of the ratio of grain size to layer thickness. Under general experimental conditions, $G_c' \simeq G_c$ since $a \ll 1$. The failure condition implies that G_c' is compensated for the energy of the bond that was broken at the crack tip. We note that $P(t)$ also appears in the condition. This is because crack progression changes the local state at the crack tip to an isotropic stress state, as $P(t)$ acts on the crack surface as well as on the top surface, as indicated in eq. (11).

5. Analytical Solution for Steady Growth

Elastic energy is stored when the compressive stress $P(t)$ increases and is dissipated by plastic relaxation. Thus, cracks can use only the remaining energy for growth. The uniform solution of eq. (10) for the initial conditions $\mathbf{s}_j(x, 0) = \mathbf{0}$ represents a state far in advance of a growing crack. By assuming

that $U_j(x, t) = 0$ everywhere, we can obtain the uniform solution

$$\mathbf{s}_j(x, t) = (0, P(t) - (\tau_p + 1)v_p(t), 0) \equiv \mathbf{s}_u(t), \quad (16)$$

where

$$v_p(t) \equiv \frac{1}{\tau_p + 1} \int_0^\infty d\eta \, [P(t) - P(t - (\tau_p + 1)\eta)] \, e^{-\eta}. \quad (17)$$

The remaining elastic energy is determined by $v_p(t)$, and $\tau_p v_p(t)$ then provides the driving force for the crack, as will be shown later. When $P(t)$ increases monotonically,

$$\begin{cases} \tau_p v_p \simeq \tau_p \dot{P} & \text{for } \tau_p \dot{P} \ll P, \\ \tau_p v_p \simeq P & \text{otherwise,} \end{cases} \quad (18)$$

as Fig. 5 indicates. For example, if $P(t)$ increases linearly from zero,

$$v_p(t) = \dot{P} \left(1 - e^{-\frac{P(t)}{(\tau_p+1)\dot{P}}} \right) \quad (19)$$

for $t > 0$ and a given increasing rate $\dot{P}$.

For a given constant v_p, the analytical solution can be obtained for the steady growth of a semi-infinite crack. We introduce the moving coordinate $\xi \equiv x - X(t)$ determined by crack growth at a constant speed $V \equiv \dot{X}$, and rewrite the basic eqs. (9)-(15) using the new variables, $\mathbf{s}'_j \equiv \mathbf{s}_j - \mathbf{s}_u$ and $\mathbf{S}'_j \equiv (1 + \partial/\partial t)\mathbf{s}'_j = (S_{xj}, S_{yj} - P + \tau_p v_p, S_{zj})$. In eqs. (9) and (13), $\mathbf{S}_j$ and x are simply replaced with $\mathbf{S}'_j$ and ξ, respectively. The other equations are altered as follows:

$$\mathbf{S}'_j - \tau_p V \frac{\partial \mathbf{s}'_j}{\partial \xi} = \left(\frac{\partial U_j}{\partial \xi}, \frac{U_{j+1} - U_j}{a}, U_j \right), \quad (20)$$

$$\sigma' = \begin{cases} \frac{2U_1}{a} - S'_{y0} & \text{for } \xi \geq 0 \\ -\tau_p v_p & \text{for } \xi \leq 0 \end{cases}, \quad (21)$$

$$\frac{a}{4} \left[\frac{2u_1}{a} - s'_{y0} + (\tau_p + 1)v_p \right]^2 = G'_c \quad \text{at } \xi = 0, \quad (22)$$

where

$$\sigma' \equiv \frac{U_2 - U_1}{a} - S'_{y1} + a \left(\frac{\partial^2 U_1}{\partial \xi^2} - \frac{\partial S'_{x1}}{\partial \xi} - U_1 + S'_{z1} \right). \quad (23)$$

These equations do not contain $P(t)$ explicitly.

We can solve these equations by the Wiener-Hopf method[16] (summarized in Appendix B) to obtain the crack speed (B·15). For $\tau_p \gg 1$ and $a \ll 1$, we find that the crack grows when $\tau_p v_p > \tau_p v_p^* \simeq \sqrt{2G'_c}$, and the growth speed is determined by

$$V \simeq \frac{a}{2} \left[\left(\frac{v_p}{v_p^*} \right)^2 - 1 \right] \quad (24)$$

for $v_p^* < v_p \ll v_p^* \sqrt{2/a}$. Combined with eq. (18), eq. (24) indicates that the crack speed is determined by $\dot{P}$ for $\tau_p \dot{P} \ll P$, and that cracks can grow only when $\dot{P} > v_p^*$, as the maximum v_p is $\dot{P}$.

These results qualitatively agree with the features of crack growth that were observed in our experiments. In particular, in the case where v_p^* is sufficiently smaller than $\dot{P}$, the onset of growth is determined by P, while the crack speed depends on $\dot{P}$, rather than on P. Returning to the original scales, cracks

start growing at a certain critical pressure,

$$P^* \simeq \tau_p v_p^* \simeq \left(\frac{2G_c \sqrt{K\mu}}{h} \right)^{\frac{1}{2}}, \quad (25)$$

and then accelerate to the speed

$$V \simeq \sqrt{\frac{\mu}{K}} \frac{a_y}{2\tau} \left[\left(\frac{\tau_p \dot{P}}{P^*} \right)^2 - 1 \right], \quad (26)$$

as $P(t)$ increases beyond $\tau_p \dot{P}$.

6. Numerical Simulations for Finite Yield Stresses

We carried out numerical simulations to confirm the analytical results and investigate the effect of finite yield stresses. Here, we assume Bingham-type constitutive equations for individual network connections in the x-, y-, and z-directions, replacing eq.(10) with

$$\tau_p \dot{\mathbf{s}}_j = (Y(f_{xj}), Y(f_{yj}), Y(f_{zj})), \quad (27)$$

$$Y(x) \equiv \begin{cases} x - F_c & \text{for } x > F_c \\ 0 & \text{for } |x| < F_c \\ x + F_c & \text{for } x < -F_c \end{cases}.$$

This is equivalent to replacing $\tau_p \dot{\mathbf{s}}_j^2$ with $\tau_p \dot{\mathbf{s}}_j^2 + F_c(|\dot{s}_{xj}| + |\dot{s}_{yj}| + |\dot{s}_{zj}|)$ in eq. (7). Here, we assumed that yielding is a purely dynamic effect;[8] that is, the functions of F_b and v are independent of F_c.

For a monotonically increasing $P(t)$ exceeding F_c, the uniform solution of eq. (27) approaches

$$\mathbf{s}_j = (0, P(t) - F_c - (\tau_p + 1)v_p, 0) \quad (28)$$

with time. For finite yield stresses and $\tau_p \gg 1$, we therefore expect that $\tau_p v_p + F_c$ provides the driving force for steady growth in place of $\tau_p v_p$.

In the numerical simulations, we solved the basic equations eqs.(8), (9), (27), and (11)-(15) in a rectangular moving region with $-L_x < \xi < L_x$ and $0 < y < L_y$. Equation (9) was solved directly by calculating the inverse matrix,[17] and eq. (27) was solved by the Euler method with the time mesh Δt, which was changed adaptively so that the intervals of successive crack progressions were longer than $4\Delta t$. The uniform solution was also calculated to obtain the boundary condition ahead of the crack. The crack progression times at the tip were obtained from eq. (12) with accuracy on the order of $(\Delta t)^2$, and for every crack progression, all fields were translated by $-\Delta x$ in the x-direction, using parabolic interpolation. For the sake of achieving good numerical performance, we again discretized the equations on a rectangular perimeter lattice with $(2I + 1) \times J$ grids, where the grid size increased exponentially as $\Delta x_i \times \Delta y_j \simeq \Delta x e^{|i-I|/4} \times a e^{j/4}$ from $\Delta x \times a$ at the crack tip $(i, j) = (I, 0)$.

All the results in Figs. 6 and 7 were obtained for $a = 0.02$, $\Delta x = 0.002$, $\tau_p = 100$, and $(I, J) = (24, 18)$, which corresponds to the system size $(L_x, L_y) \simeq (5.0, 4.9)$. We have assumed that $4G'_c/a = 1$ by choosing an appropriate scaling constant u.

Figure 6 shows the time development of the crack tip position under a linearly increasing pressure $P = \dot{P}t$ $(t \geq 0)$ for $F_c = 0$ and $F_c = 1$. These are consistent with the analytical results shown in §5. For $F_c = 0$, cracks can grow only for large $\dot{P}$, and the crack speed settles into the value determined
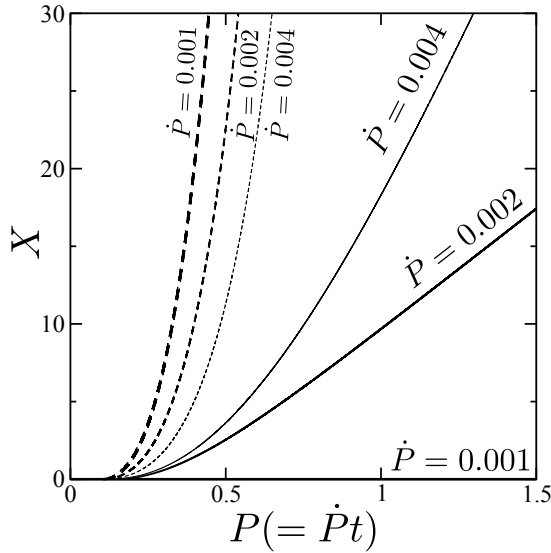
Fig. 6. Crack tip positions $X(t)$ for linearly increasing pressures $P(t)$. Solid and dashed lines represent the respective numerical results in zero yield stress ($F_c = 0$) and nonyielding cases ($F_c = 1$).

Fig. 7. Growth speeds at a given X are plotted with respect to P for $F_c = 1$ and with respect to $\tau_p v_p$ in the other cases. $\tau_p v_p$ is given by eq. (19) for linearly increasing $P(t)$, and is calculated using eq. (28) for decreasing dP/dt.

by $\dot{P}$. On the other hand, for $F_c = 1$, cracks always grow for $\dot{P} > 0$, and the speed increases as the pressure increases. At the onset of crack growth, the pressure is approximately the same in all cases.

$F_c = 1$ corresponds to purely viscoelastic cases, as plastic deformation is absent virtually everywhere. Hence, the results agree with what occurs when $\tau_p \to \infty$. In this case, the driving force of crack growth is the pressure $P(t)$, which is $\tau_p v_p$ for $\tau_p \to \infty$.

Figure 7 shows the crack speed with respect to $\tau_p v_p(t)$ or $P(t)$. The results for $F_c = 0$ and $F_c = 1$ were obtained for a linearly increasing $P(t)$, as shown in Fig. 6. The data are plotted with respect to $\tau_p v_p(t)$ for $F_c = 0$ and with respect to $P(t)$ for $F_c = 1$. Both sets of data agree with the theoretical curve obtained using eq. (24) represented by the dotted line. Thus, we have confirmed that the crack speed is determined by $\tau_p v_p$, which depends on $\dot{P}$ in viscoplastic cases, and corresponds to P in viscoelastic cases.

Crack growth is faster for finite yield stresses than for $F_c = 0$, and exhibits hysteresis. In Fig. 7, the results are plotted with respect to $\tau_p v_p(t)$ for $F_c = 0.2$. Under conditions of linearly increasing pressure, cracks can grow only when $\tau_p v_p$ is larger than 0.03 (indicated by the arrow), and long distances are required to achieve stationary growth. On the other hand, the crack speed decreases continuously with $\tau_p v_p$ when $dP(t)/dt$ decreases gradually, as indicated by the solid line in Fig. 7. This line corresponds approximately to the crack speed in the stationary state. We confirmed that this line is in close agreement with the theoretical curve obtained using eq. (24) by applying a parallel shift of $F_c = 0.2$ along the $\tau_p v_p$ axis.

7. Discussion and Conclusions

In conclusion, the competition between two stress relaxation mechanisms (crack growth and plastic deformation) causes the drying rate dependence of crack growth. Cracks in paste that is subject to linear plastic relaxation grow when
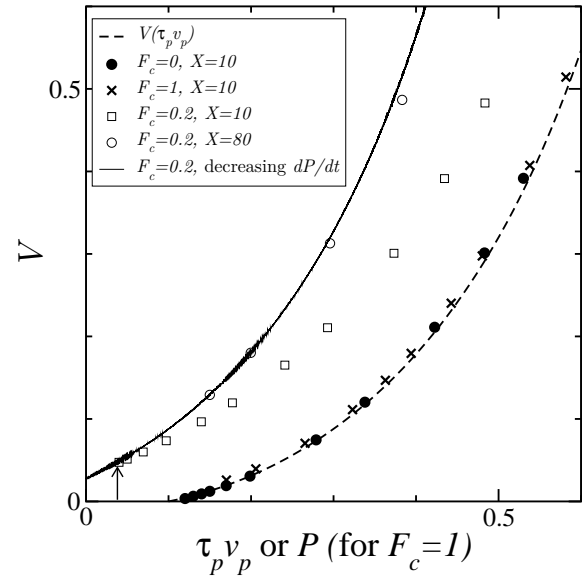
$\tau_p \dot{P}$ is larger than the critical value v_p^*, and the speed is determined by $\tau_p \dot{P}$ using eq. (24) or (26) in our model. For a large τ_p, the transient region exhibits viscoelastic growth before settling into steady propagation, in which cracks accelerate as pressure increases beyond a critical pressure $P^* \simeq v_p^*$. Finite yield stresses allow cracks to grow for smaller values of $\dot{P}$ as F_c increases. Under steady propagation, the crack speed is determined by replacing $\tau_p \dot{P}$ with $\tau_p \dot{P} + F_c$ in eq. (26), and the crack growth changes to viscoelastic for large F_c values. These results are qualitatively consistent with the results of our experiments.

A quantitative comparison with the experimental results is difficult at present owing to a lack of information on the mechanical properties of paste during crack formation. μ, K, τ_p, and F_c generally increase with drying. Rheological measurements for various water volume fractions will yield the values of μ/K and τ in the viscoelastic region, and those of τ_p and F_c in the plastic region.

The results of our experiments on $CaCO_3$ paste suggest that F_c was close to P^* at the onset of crack formation. Cracks were estimated to occur at $P^* = 10^4 - 10^5$ Pa in the range of the rate of pressure increase, $\dot{P}(v_f(t)) = P'(v_f)\dot{v_f} = 2 - 120$ Pa/s, where v_f is the water volume fraction. On the other hand, the relaxation time τ_p should have been less than 10 s, as the cracks stopped growing as soon as further desiccation was prevented by covering the container with a lid.[9] Therefore, we infer that $\tau_p \dot{P} \ll P^*$, and $F_c \simeq P^*$ is then required in order for cracks to grow. Although it is beyond the scope of this study to investigate the relationship between F_c and P^*, the modified form of eq. (26) for a finite yield stress can be approximated by

$$V \simeq \sqrt{\frac{\mu}{K}} \frac{a_y}{2\tau} \left[\left(\frac{\tau_p \dot{P} + F_c}{P^*} \right)^2 - 1 \right] \simeq \sqrt{\frac{\mu}{K}} \frac{a_y}{\tau} \frac{\tau_p \dot{P}}{F_c}, \quad (29)$$

if $F_c \simeq P^*$. Hence, V is expected to show a linear dependence

on $\dot{P}$. Our experiments indicated a weaker nonlinear dependence of V on $\dot{P}$. This discrepancy may be due to the simplification used to construct F_p and v, and the assumption of Bingham-type plasticity. Although our spring-network-based model has been used intuitively in qualitative discussion, a more accurate theory is required.

In addition to viscoelastic fracture and quasi-static fracture controlled by water distribution, in this paper, we suggested a new type of fracture in which cracks grow dynamically by competing with global plastic relaxation. Some experiments have indicated that crack speed varies significantly depending on the material composition of the paste. It would be interesting in future studies to investigate whether this variation is responsible for the crack growth type.

Acknowledgments

Appendix A: Derivation of the basic equations

The summation in eqs. (4) and (5) must be handled carefully, so that elements in the crack are excluded. For example, the sum in eq. (4) is defined as

$$\int dx \sum_j{}' a\mathbf{e}_j^2 \equiv \int_{-\infty}^{\infty} dx \sum_{j=1}^{\infty} a\mathbf{e}_j^2 + \frac{a}{2}\int_{X(t)}^{\infty} dx e_{y0}^2 \qquad (A\cdot 1)$$

for the half plane $y > 0$. The time derivative

$$\frac{d}{dt}\int dx \sum_j{}' a\mathbf{e}_j^2 = 2\int dx \sum_j{}' a\mathbf{e}_j \cdot \dot{\mathbf{e}}_j - \frac{a}{2} e_{y0}^2\big|_{x=X}\dot{X} \quad (A\cdot 2)$$

is substituted into eq. (1), and the same procedure is performed for eq. (5). The coefficients of $\dot{u}_j$, $\dot{s}_j$, and $\dot{X}$ are obtained from eq. (7) after integrating by parts, as follows:

$$\int dx \sum_j{}' a\mathbf{e}_j \cdot \left(\frac{\partial\dot{u}_j}{\partial x}, \frac{\dot{u}_{j+1}-\dot{u}_j}{a}, \dot{u}_j\right)$$

$$= -\int_{-\infty}^{\infty} dx \sum_{j=2}^{\infty}\left(a\frac{\partial e_{xj}}{\partial x} + e_{yj} - e_{yj-1} - ae_{zj}\right)\dot{u}_j$$

$$-\int_{-\infty}^{\infty} dx \left(a\frac{\partial e_{x1}}{\partial x} + e_{y1} - ae_{z1} - e_{y0}\Theta(x-X)\right)\dot{u}_1, \quad (A\cdot 3)$$

where $\Theta(t)$ is the Heaviside step function. Here, we used the boundary conditions (8).

Appendix B: Wiener-Hopf analysis

We apply the Fourier transform defined by

$$\hat{X}(k) \equiv \frac{1}{2\pi}\int_{-\infty}^{\infty} d\xi X(\xi)e^{-ik_\epsilon\xi}, \quad k_\epsilon \equiv k + i\epsilon, \qquad (B\cdot 1)$$

for a small positive ϵ. ϵ is ultimately made to approach zero. From the definition of $(U_j, \mathbf{S}'_j)$, $(\hat{U}_j, \hat{\mathbf{S}}'_j) = (1 - ik_\epsilon V)(\hat{u}_j, \hat{s}'_j)$ in the moving coordinate system, and $\hat{U}_0 = -\hat{U}_1$ from the boundary conditions (8).

Our basic equations are transformed as follows:

$$\hat{\mathcal{L}}\hat{U}_j = \frac{\hat{S}'_{yj} - \hat{S}'_{yj-1}}{a} + ik_\epsilon\hat{S}'_{xj} - \hat{S}'_{zj}, \qquad (B\cdot 2)$$

$$a\hat{\mathbf{S}}'_j - i\tau_p Vk_\epsilon a\hat{\mathbf{s}}'_j = (ik_\epsilon a\hat{U}_j, \hat{U}_{j+1} - \hat{U}_j, a\hat{U}_j), \qquad (B\cdot 3)$$

$$\begin{cases} a\hat{\sigma}' - 2\hat{U}_1 + a\hat{S}'_{y0} = -2U_+(k) \\ \hat{\sigma}' - \frac{\tau_p v_p}{2\pi ik_\epsilon} = T_-(k) \end{cases}, \qquad (B\cdot 4)$$

$$\int_{-\infty}^{\infty} dk\left(\frac{2\hat{u}_1}{a} - \hat{s}'_{y0}\right) + (\tau_p + 1)v_p = \sqrt{\frac{4G'_c}{a}}, \qquad (B\cdot 5)$$

where $a^2\hat{\mathcal{L}}\hat{U}_j \equiv \hat{U}_{j+1} + \hat{U}_{j-1} - (2 + z^2)\hat{U}_j$, $a\hat{\sigma}' \equiv \hat{U}_2 - (1 + z^2)\hat{U}_1 - a\hat{S}'_{y1} + a^2(\hat{S}'_{z1} - ik_\epsilon\hat{S}'_{x1})$, and $z^2 \equiv a^2(k_\epsilon^2 + 1)$. U_+ and T_- are undetermined complex functions, and the subscripts $+$ and $-$ indicate that they are analytic for $\mathrm{Im}\,k > 0$ and $\mathrm{Im}\,k < 0$, respectively.

We first obtain

$$a\hat{\mathbf{S}}'_j = (1 - \hat{T}_p^{-1})(ik_\epsilon a\hat{U}_j, \hat{U}_{j+1} - \hat{U}_j, a\hat{U}_j),$$

$$\hat{T}_p \equiv 1 + \frac{1}{\tau_p} - \frac{1}{i\tau_p k_\epsilon V}, \qquad (B\cdot 6)$$

from eq. (B·3) to eliminate $\hat{\mathbf{S}}'_j$ and $\hat{\mathbf{s}}'_j$ from the other equations. Equation (B·2) is changed to $\hat{\mathcal{L}}\hat{U}_j = 0$, and its eigenvalue equation $e^{-\lambda a} + e^{\lambda a} - 2 - z^2 = 0$ is obtained by assuming that $\hat{U}_j \equiv \hat{U}_1 e^{-\lambda a(j-1)}$ for $j > 0$.

Eliminating $\hat{U}_1$, the boundary conditions (B·4) are reduced to a single equation

$$-\alpha(k)U_+(k) = \frac{\tau_p v_p}{2\pi ik_\epsilon} + T_-(k), \qquad (B\cdot 7)$$

where

$$\alpha(k) \equiv \frac{2}{a}\frac{e^{-\lambda a} - 1 - z^2}{e^{-\lambda a} - 3 - z^2} = \frac{2}{a}\left(\frac{z^2}{z^2 + 4}\right)^{\frac{1}{2}}. \qquad (B\cdot 8)$$

The WH decompositions into half-space analytic functions, $\alpha(k) = \alpha_+(k)\alpha_-(k)$ and

$$h(k) \equiv -\frac{\tau_p v_p}{2\pi i\alpha_- k_\epsilon} = h_+(k) + h_-(k), \qquad (B\cdot 9)$$

yield the solution

$$U_+(k) = \frac{h_+(k)}{\alpha_+(k)} \quad \text{and} \quad T_-(k) = h_-(k)\alpha_-(k) \qquad (B\cdot 10)$$

since $\alpha_+ U_+ - h_+ = h_- - \frac{T_-}{\alpha_-} = 0$ by Liouville's theorem and the stress continuity requirement at the crack tip for $a > 0$.

The decompositions are given explicitly by

$$\alpha_\pm(k) = \left(\frac{2}{a}\frac{1 \mp ik_\epsilon}{b \mp ik_\epsilon}\right)^{\frac{1}{2}}, \qquad (B\cdot 11)$$

$$h_+(k) = -\frac{1}{2\pi i}\oint_{k_\epsilon = 0} dk'\frac{h(k')}{k' - k} = -\frac{\tau_p v_p}{2\pi i\alpha_-(-i\epsilon)k_\epsilon}, \quad (B\cdot 12)$$

and $h_-(k) = h(k) - h_+(k)$, where $b \equiv \sqrt{1 + 4/a^2}$.

The crack speed is obtained by substituting these expressions into the failure condition (B·5). We then integrate

$$\frac{2\hat{u}_1}{a} - \hat{s}'_{y0} = \frac{2}{a}\frac{\hat{T}_p^{-1}\hat{U}_1}{1 - ik_\epsilon V} = \frac{(\frac{2}{a} - \alpha)U_+}{1 - ik_\epsilon V} \qquad (B\cdot 13)$$

using the residue theorem and obtain

$$\int_{-\infty}^{\infty} dk \left(\frac{2\hat{u}_1}{a} - \hat{s}'_{y0} \right) = \tau_p v_p \left(-1 + \frac{\alpha_-(-\frac{i}{V} - i\epsilon)}{\alpha_-(-i\epsilon)} \right). \quad (B\cdot14)$$

Substituting eq. (B·11), eq. (B·5) becomes

$$v_p \left(\tau_p \sqrt{\frac{V+1}{V+\frac{1}{b}}} + 1 \right) = \sqrt{\frac{4G'_c}{a}} \quad (B\cdot15)$$

in the limit as $\epsilon \to 0$.

1) A. Groisman and E. Kaplan: Europhys. Lett. **25** (1994) 415.
2) G. Müller and T. Dahm: J. Geophys. Res. **105** (2000) 723.
3) G. Müller: J. Struct. Geol. **23** (2001) 45.
4) S. Kitsunezaki: Phys. Rev. E **60** (1999) 6449.
5) P. Coussot: *Rheometry of Pastes, Suspensions, and Granular Materials* (John Wiley & Sons, Hoboken, New Jersey, 2005).
6) A. Nakahara and Y. Matsuo: J. Phys. Soc. Jpn. **74** (2005) 1362; Phys. Rev. E **74** (2006) 045102(R); J. Stat. Mech. (2006) P07016.
7) M. Otsuki: Phys. Rev. E **72** (2005) 046115.
8) T. Ooshida: Phys. Rev. E **77** (2008) 061501; J. Phys. Soc. Jpn. **78** (2009) 104801.
9) S. Kitsunezaki: J. Phys. Soc. Jpn. **78** (2009) 064801.
10) N. Mitarai and F. Nori: Adv. Phys. **55** (2006) 1.
11) D. M. Wood: *Soil Behaviour and Critical State Soil Mechanics* (Cambridge University Press, New York, 1990).
12) K. B. Singh and M. S. Tirumkudulu: Phys. Rev. Lett. **98** (2007) 218302.
13) W. Man and W. B. Russel: Phys. Rev. Lett. **100** (2008) 198302.
14) L. Pauchard, B. Abou, and K. Sekimoto: Langmuir **25** (2009) 6672.
15) B. Lawn: *Fracture of Brittle Solids* (Cambridge Univ. Press, Cambridge, 1993) 2nd ed.
16) L. B. Freund: *Dynamic Fracture Mechanics* (Cambridge University Press, New York, 1990).
17) uBLAS, C++ linear algebra library (http://www.boost.org) was used.